Relative stabilities of metastable states of convecting charged-fluid systems by computer simulation

PHYSICAL REVIEW A VOLUME 27, NUMBER 1 JANUARY 1983

Relative stabilities of metastable states of convecting charged-fluid systems by computer simulation

Makoto Suzuki* and Yasuji Sawada
Research Institute of Electrical Communication, Tohoku University, Sendai 980, Japan
(Received 26 April 1982)

Dissipative structures in charged-fluid layer systems have been investigated by computer simulations. In a supercritical condition the system takes a convective state. It was found that the steady convective states were highly degenerate and one of the states gave the maximum charge transport. Relative stabilities of such metastable states were examined by disturbing each state. These investigations revealed that the most stable convective state corresponded to the state of maximum charge transport within the computational error, supporting the maximum-entropy-production hypothesis for a multi-stable-state system.

I. INTRODUCTION

In a far from equilibrium condition a system organizes itself spontaneously into a state with a spatial or temporal structure. It is called a dissipative structure in contrast to the structure in thermodynamic equilibrium. Bénard convection, Couette flow, growing dendritic cyrstals, Belousov-Zhabotinski reaction system, and oscillating chemical or biochemical reactions such as glycolic cycles are well-known examples of dissipative structures.[1] They may be classified into either spatial structures or temporal structures, or their combinations. Nonequilibrium thermodynamics has been developed extensively in the last two decades especially by Prigogine and his co-workers.[2] Their arguments on the stability of nonequilibrium states with the assumpiton of local equilibrium has brought some essential results: the theorem of excess entropy production for a stable state and the general evolution criterion for general nonlinear processes. These consequences were obtained by taking into account small fluctuations around a reference state. Although these theorems were in part criticized,[3] they are certainly a landmark of the nonequilibrium thermodynamics.

If the magnitude of the fluctuations is not small, the state of the system may be transferred to another state, if it exists, and the new state may be more stable against perturbation. The theorems cited above are not helpful to tell us which are the most stable states among the others. Therefore, the thermodynamic principle governing the relative stability of nonequilibrium metastable states is an important problem. The problem of relative stability generally arises when one considers nonlinear, nonequilibrium systems which have steady multistable states.

For Bénard convection, Malkus and Veronis[4] proposed that the state of the maximum heat transfer is the most stable among the states of structures with possible wave numbers from an analysis near the critical point for Bénard instability. Roberts[5] has shown that the wave number of the mode corresponding to the maximum heat transport was close to that of fluctuation with the maximum rate of evolution from a reference steady state. Felici[6] has proposed intuitively from his experience the principle of facilitation, by which he means that a nonequilibrium system tends to select one of the easiest flow states. Independently, Sawada[7] has recently demonstrated from a thermodynamic argument including reservoirs that the most stable states against perturbation among the multisteady states should correspond to the state of the maximum entropy production, and that even a nonequilibrium nonsteady state should select a mode with the entropy-production maximum, if some condition on time scales is satisfied. It would therefore be important to examine whether the principle stated above is supported by the results of experiments or by the numerical computation for nonlinear, nonequilibrium processes.

Among nonlinear, nonequilibrium systems, charged viscous fluids present several interesting dissipative structures such as Felici convection,[8] nonlinear oscillations of ion drap pumping,[9] or of ion transportation in a living cell membrane.[10] In contrast to thermal fluids, there are fewer investigations of charged fluids as systems presenting dissipative structures. Moreover, it stimulates interest since the acting force in a charged fluid is different from that in a thermal system. One difference is the nearly linear buoyant gravitational force, while the other is the nonlinear Coulomb force. The criterion

for Felici instability was shown by Atten and Moreau[11] by a linear analysis and lately confirmed by Schneider and Watson.[12] Near the critical point Lacroix[13] showed in relief the existence of hystereses in the I–V characteristics.

Atten and Lacroix[14] analyzed roll-type structures and hexagon-type structures for steady-state electroconvection near the critical point. They discussed the relative stability between the rolls and hexagonal cells in this region. The horizontal nonlinearities, however, are not fully taken into account in this method, especially in transient processes.

Further interests are on the multisteady states, namely metastable states, the relative stability, and the transition processes among them. We shall show the results of a numerical analysis including sufficient nonlinearity to progress understanding of these problems.

II. SIMULATION OF ELECTROCONVECTION

Let us consider the case in which unipolar charges are injected uniformly into an incompressible isotropic viscous insulating liquid layer subject to a uniform potential difference V_0 across it. The fluid motion is governed by the conservation laws of mass, momentum, charge, the Poisson equation, and the equation of fluid states. For an incompressible fluid the basic equations are given in terms of dimensionless variables as

$$x_i' = x_i/d, \quad t' = t\kappa V_0/d^2, \quad \vec{E}' = \vec{E}d/V_0 ,$$

$$\Phi' = \Phi/V_0, \quad \epsilon' = \epsilon/\bar{\epsilon}, \quad q' = qd^2/\epsilon V_0 ,$$

$$\vec{j}' = \vec{j}d^3/\epsilon\kappa V_0^2, \quad p' = pd^2/\rho\kappa^2 V_0^2 ,$$

and

$$\vec{u}' = \vec{u}d/\kappa V_0 ,$$

where x_i represents the i component of coordinate x, d the layer thickness, t the time, κ the charge mobility, V_0 the potential difference, $\vec{E}$ the electric field, Φ the electric potential, ϵ the dielectric constant of the fluid, $\bar{\epsilon}$ the average dielectric constant, q the charge density, j the current density, p the pressure, ρ the density, and $\vec{u}$ the fluid velocity. Deleting the prime from all variables, they are written as

$$\vec{\nabla}\cdot\vec{u} = 0 , \tag{1}$$

$$\frac{\partial\vec{u}}{\partial t} + \vec{u}\cdot\vec{\nabla}\vec{u} = -\vec{\nabla}p + \frac{1}{R_e}\Delta\vec{u} + M^2F_e , \tag{2}$$

$$\frac{\partial q}{\partial t} + \vec{\nabla}\cdot\vec{j} = 0 , \tag{3}$$

$$\vec{j} = g(\vec{E}+\vec{u}) , \tag{4}$$

$$q = \vec{\nabla}\cdot\vec{E} , \tag{5}$$

$$\vec{E} = -\vec{\nabla}\Phi , \tag{6}$$

$$F_e = q\vec{E} - \tfrac{1}{2}E^2\vec{\nabla}\epsilon + \vec{\nabla}\left[\frac{\rho}{2}\left[\frac{\partial\epsilon}{\partial\rho}\right]E^2\right] . \tag{7}$$

Here $M = (\epsilon/\rho)^{1/2}\kappa$ is an important parameter for charge transportation in a fluid, since it is the ratio of hydrodynamic mobility and carrier mobility. $R_e = \kappa V_0/\nu$ is the electric Reynolds number, where ν is the kinematic viscosity. It is convenient to introduce a parameter $T = M^2R_e$ which is analogous to the Rayleigh number in Bénard convection, so that it can be called the electric Rayleigh number. Equation (1) represents the law of mass conservation for an incompressible fluid, Eq. (2) the law of momentum conservation, namely, Navier-Stokes equation for a Newtonian fluid, Eq. (3) the charge conservation law, Eq. (4) the total current density consisting of conductive and convective currents, Eqs. (5) and (6) the Poisson equation, and Eq. (7) the electric force density. Since we consider the case of slow motions of substances and small carrier density, we neglect the effect of magnetic fields. In Eq. (7) the second term in the right-hand side can be separated into two terms as

$$\vec{\nabla}\epsilon = \left[\frac{\partial\epsilon}{\partial\rho}\right]_{T_m}\vec{\nabla}\rho + \left[\frac{\partial\epsilon}{\partial T_m}\right]_{\rho}\vec{\nabla}T_m ,$$

where T_m is the temperature. We considered the case where the heat generated due to the Joule effect and viscous dissipations can be neglected. The temperature is then uniform in the liquid layer. Therefore, the second term in Eq. (7) is omitted. The third term can be gathered with the gradient term of Eq. (2) which can be eliminated by a rotation operation. Therefore, the effective electric force is the first term in Eq. (7). It is noted that when charge carriers move along the electric field, the time required to attain the steady velocity after many collisions with liquid molecules is much shorter than the characteristic time for the macroscopic liquid motion. It means that the force acting on carriers is instantaneously transmitted to the liquid from the external field.

Two kinds of analysis may be considered. One is performed in real space, and the other in wave number space. A merit of the latter is the possibility of determining the boundary conditions precisely and approximating the distributions of variables with comparatively few variables, namely, Fourier coefficients.

In the case that the nonlinear terms play an important role, the truncation error of higher-order coefficients becomes significant. If the distributions

of physical variables are represented with Fourier series both in vertical and horizontal directions, there appears a considerable number of coefficients. On the other hand, when real-space difference equations are analyzed, there are physical variables corresponding to each space point. Nevertheless, the best feature of the real-space analysis is to enable simulations of continuous deformation of structure in any direction without truncation errors.

In the present work the analysis was made with the Ψ-ω method. In Eq. (2) the gradient term was eliminated by applying rotation. By introducing the stream function Ψ and vorticity $\omega=(0,\omega,0)$ Eq. (2) becomes

$$\frac{\partial\omega}{\partial t}=-\left[\frac{\partial\Psi}{\partial z}\frac{\partial\omega}{\partial x}-\frac{\partial\Psi}{\partial x}\frac{\partial\omega}{\partial z}\right]+\frac{1}{R_e}\Delta\omega +M^2\left[-\frac{\partial q}{\partial z}\frac{\partial\Phi}{\partial x}+\frac{\partial q}{\partial x}\frac{\partial\Phi}{\partial z}\right], \tag{8}$$

where

$$\vec{\omega}=\vec{\nabla}\times\vec{u}\ ,$$

$$\vec{u}=\left[\frac{\partial\Psi}{\partial z},0,\frac{-\partial\Psi}{\partial x}\right],$$

$$\Delta\Psi=\omega\ . \tag{9}$$

Rewriting Eqs. (3)—(6) yields

$$\frac{\partial q}{\partial t}=-\vec{\nabla}\cdot[q(\vec{E}+\vec{u})]\ , \tag{10}$$

$$\Delta\Phi=-q\ . \tag{11}$$

Thus this system consists of two dynamic equations and two Poisson equations. The boundary conditions are shown below.

Our system is a two-dimensional cell with a rectangular cross section of the aspect ratio of ten. Unipolar charges are injected uniformly into the insulating liquid layer with a fixed density at the lower electrode plate, namely, the injector. The upper electrode is the collector. The side walls are rigid and electrically insulating. The space to be calculated is divided into a thousand equal squares (vertically by ten and horizontally by a hundred divisions) with the side length $h=0.1$.

A set of finite difference equations corresponding to Eqs. (1)—(7) must satisfy the following requirements. First, the law of causality concerning the convective transport of perturbations, and second, the conservation laws of mass and energy. Unless one considered the transient phenomena, the first requirement is not necessary. We are, however, interested in both transient phenomena and steady states. We tried two schemes, the upstream difference scheme and the central difference scheme, for the vorticity calculation. The former scheme satisfies the above requirements with comparatively stable computation and is considered to give qualitatively correct results. The latter scheme does not, however, satisfy the first requirement, but gives more accurate steady states. One of the implicit methods, called the Crank-Nicholson method, was applied on the vorticity calculations, and the results were found to be qualitatively correct by one of the upstream methods, called the donor cell method. When the Reynolds number is small, it is expected that the central difference scheme on the vorticity calculation gives correct transient results. The donor cell method is known to have an accuracy better than first order in h.[15] On the other hand, calculation on charge q is made only by the donor cell method since the spatial variation of charge q is considered to be small compared to that of the vorticity. The implicit method with the central difference scheme for q is of course preferable, but it is too time consuming. A detailed procedure of the numerical calculation is described in the Appendix.

III. THE RESULTS OF COMPUTER SIMULATION AND DISCUSSIONS

A. The quiescent conduction state

First, the quiescent conduction state was obtained to test the accuracy of our difference scheme according to Eqs. (A1)—(A7) in the Appendix. The initial condition was the quiescent solution obtained analytically and superimposed by a sinusoidal perturbation of charge distribution with the magnitude of 1% and the wave number $k=\pi$.

For a condition of weak injection ($q_0\leq 0.5$), $q_0=0.410$, $R_e=1.0$, and $T=484$, where the critical value $T_c=1900$, the evolution of the system was investigated. At the first stage the liquid system started a convective motion, but eventually returned back to the quiescent state as shown in Fig. 1. Circles show the numerical results and the solid lines denote analytical values. The deviations were less than 0.05% for the electric potential, less than 1.00% for the charge density, and 0.03% for the mean electric current.

For a condition of intermediate injection strength ($0.5<g_0<5.0$), $q_0=2.114$ and $T=20$, where $T_c=250$, deviations extended to 1.2% in the electric potential, 20% in the charge density, and 4.5% in the mean electric current because of the steep change of charge density near the injector, which is difficult to approximate by an equal division of space. We mainly treated the weak injection case to avoid such complications.

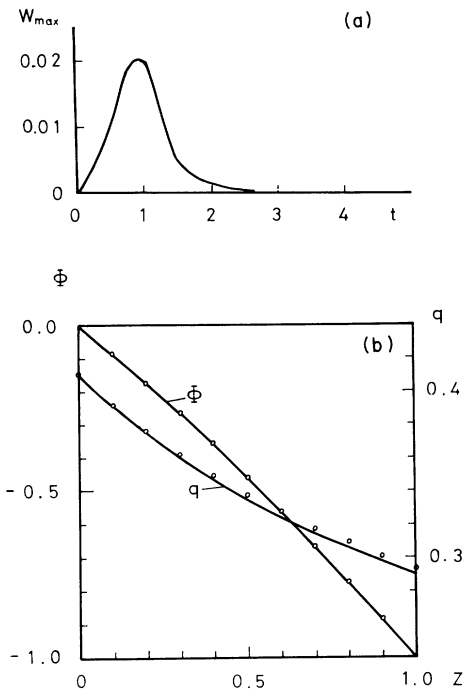

FIG. 1. Quiescent state for $q_0=0.410$ and $T=484<T_c=1900$. Solid lines are obtained analytically and open circles by computation. (a) Maximum velocity variation; (b) charge q and electric potential Φ distributions.

B. Transitions to stable structures

In a weak injection case transition processes were investigated from the initial quiescent conduction state to the fully developed convection state. Setting electric Reynolds number $T=9680$, where $T_c=1900$, $q_0=0.410$, and $M^2=484$ corresponding to nitrobenzene, the initial conduction state was modulated by sinusoidal perturbations of space charge with various wave numbers.

Two schemes were examined, one was the central difference scheme by Eq. (A1) and the other was the donor cell method, which is one of the upstream difference schemes, given by Eq. (A2) in the vorticity calculation. When R_e is small it is expected that the time developments of the system are qualitatively equal between the two schemes. If so, the former scheme should give more accurate solutions since it is accurate to h^2.

To verify this, the quiescent conductive state was initially perturbed by charge superposition with a sinusoidal distribution. The evolutions of convections by both schemes were compared both in structure and in current or entropy production. The structures were almost the same in $\Psi=0$ contours within 1% as in Fig. 2. The steady convection state

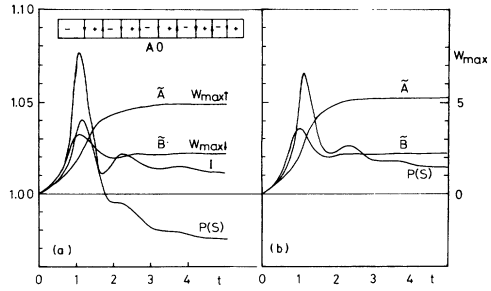

FIG. 2. Comparison of two numerical analyses. (a) Upstream scheme; (b) central difference scheme. $\tilde{A}$, upward maximum velocity; $\tilde{B}$, downward maximum velocity; I, electric current; $P[S]$, entropy production; and A0, the obtained convection structure. Only the $\psi=0$ contour is shown.

obtained by the central difference scheme is denoted as A0. During the evolution, there was no qualitative difference as shown in Figs. 2(a) and 2(b), and the central difference scheme was applied thereafter.

As the initial conditions, a cosine wave perturbation of charge density with wave number k was imposed. Time evolution of the maximum liquid velocity $W_{\max}$, the electric current I, and the entropy production $P[S]$ are shown in Fig. 3(a). The upward maximum velocities were twice as large as the downward maximum velocities. The convective motions were shown by means of contours of the stream function, where counterclockwise rotations were shown by positive signs in Fig. 3(b) above which the evolution of charge distribution was shown. The figures are symmetrical with respect to right boundaries. In this case 12 rolls were established, whose structure was denoted as A12. The region of upward flow was definitely narrower than that of downward flow and became greater in charge density. At the steady state the difference between the current and the entropy production was about 2%, which was considered to be due to the computational error, noting that $P[S]$ might be smaller than I since the central difference scheme tends to reduce spatial variations with small wavelength. Similar computations were made for various initial perturbations with wave numbers, $k=0.8\pi$, 1.0π, 1.4π, 1.6π, 1.8π, and 2.0π. Stable convection states were obtained as shown in Fig. 4 and denoted as A8, A10, A14, A16, A18, and A20, respectively. The electric current I and the maximum liquid velocity $W_{\max}$ and necessary time τ to converge to the steady state for each case were plotted in Fig. 5. There were found maximum or minimum points between 1.2π and 1.6π.

As a comparison, a computation in an intermediate injection strength, where $q_0=2.114$,

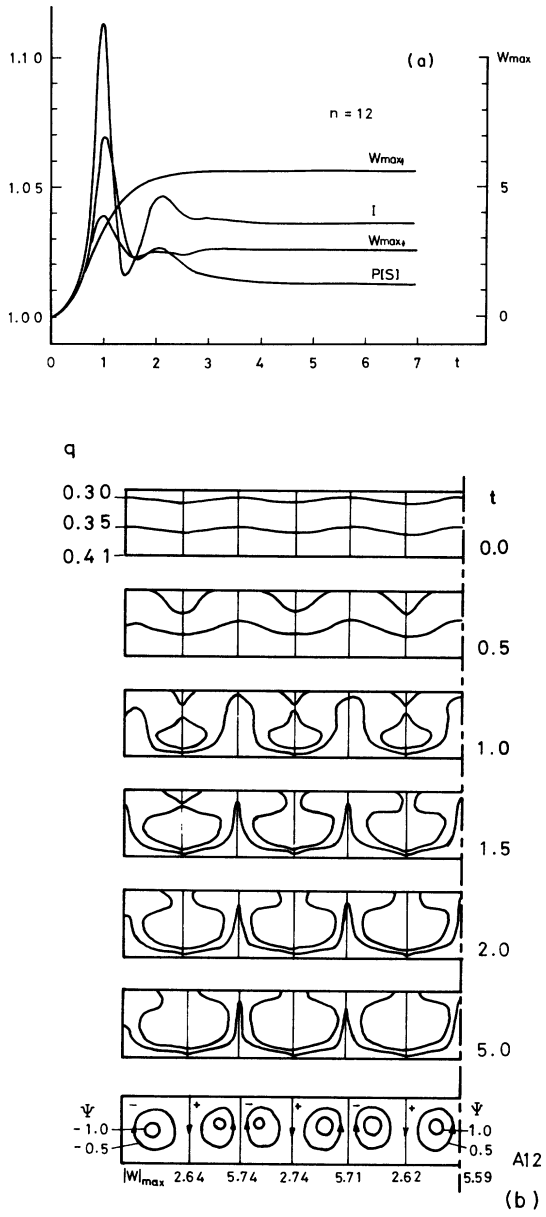

FIG. 3. Evolution of 12-roll state. (a) Current I, entropy production $P[S]$, $W_{\max\uparrow}$ and $W_{\max\downarrow}$ variations; (b) evolution of charge distribution. Bottom of (b) shows the stream lines.

$T=968>T_c=250$, was made for an initial charge perturbation of $k=2\pi$. In this case a steady stable convection was established, although there were small variations in the convective velocities. The electric Nusselt number, defined as the total electric current divided by the corresponding conduction current, was 1.22.

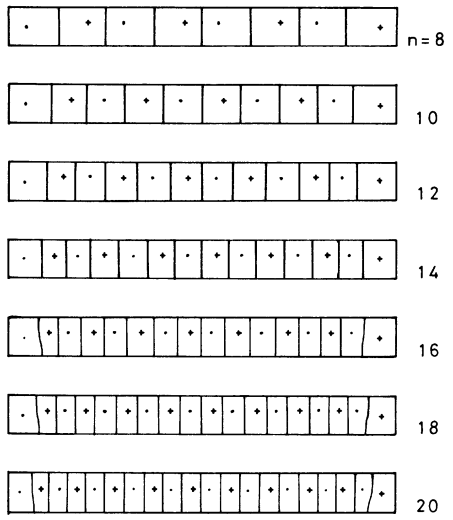

FIG. 4. Steady convective structures, A8, A10, A12, A14, A16, A18, and A20 for $q_0=0.410$, $T=9680$, $T_c=1900$. + 's denote the centers of anticlockwise rolls and dots clockwise.

C. System evolutions by initial perturbations not preferred

In a weak injection case, where $q_0=0.410$ and $T=9680$, the system did not show the simple behavior reported in the previous section where the initial perturbation was of wave number $k=2.4\pi$. In Fig. 6(a) the evolution of convection state from a quiescent state is shown. The perturbation developed as a stable structure until $t=2$; then the rolls near the side walls collapsed and the system came up to a twenty-roll structure around $t=4$. The corresponding current and the entropy production are shown in Fig. 6(b). They varied violently between $t=0$ and $t=3$ to become a relatively more stable state after $t=3.5$.

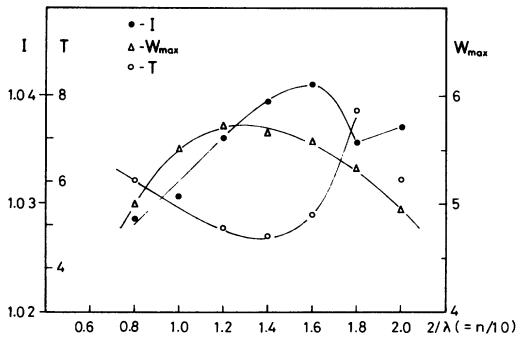

FIG. 5. Current I, maximum velocity $W_{\max}$, and converging time τ for various steady states shown in Fig. 4.

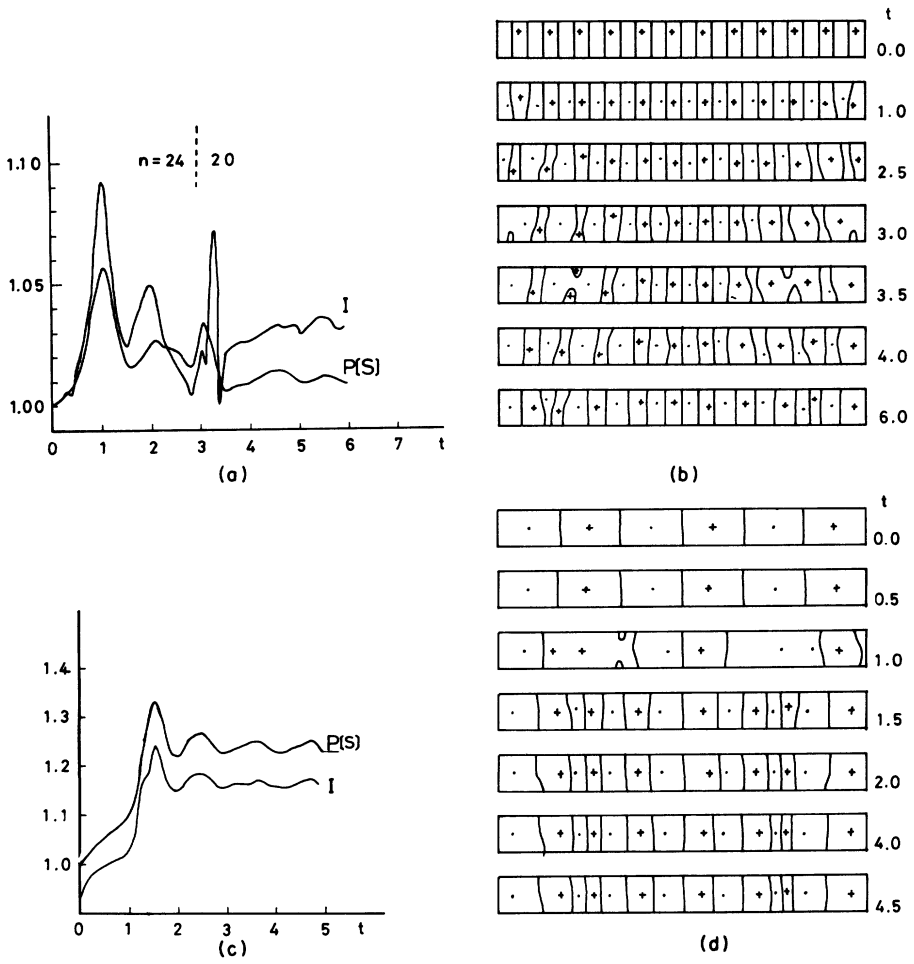

FIG. 6. Evolutions from unstable structures. (a) Twenty-four-roll state to twenty-roll state for $q_0=0.410$ and $T=9680$; (b) six-roll state to fourteen-roll state for $q_0=2.110$ and $T=968$.

In an intermediate injection strength case, where $q_0=2.114$, $T=968>T_c=250$, and the initial charge perturbation of $k=0.6\pi$, a convection state with wave number $k=0.6\pi$ developed until $t=0.5$, then the state was modified by itself to a 14-roll state as shown in Figs. 6(c) and 6(d).

In both cases the second-order derivatives of the current curves with respect to time were found to be locally negative in the growing up region. Then the structures initially given collapsed naturally and new stable structures were reconstructed.

Some comparisons are shown in Fig. 7, where circles correspond to stable convective structures, crosses for unstable structures, and solid lines for the marginally stable quiescent conduction state. The upper line is for $q_0=0.41$ and the lower line for $q_0=2.1$, obtained by interpolation from the results by Atten and Moreau.[11] The vertical axis represents the electric Rayleigh number T and the horizontal axis the wave number k. Stable convection states were found to exist in the inner regions of such lines.

D. Transitions among stable convective states by disturbances

In Sec. III A several steady stable convective states were found to exist for the same boundary condition. This implies that the states were degenerate; one might be the most stable state and the others metastable states. The liquid-layer system was considered to be transferred to a more stable state by some disturbances. We applied mainly two disturbing methods:

(1) At $t=0$ impulsive charge disturbances were applied on stable convection states. The disturbances had the following form.

(2) Different random forces were continuously ex-

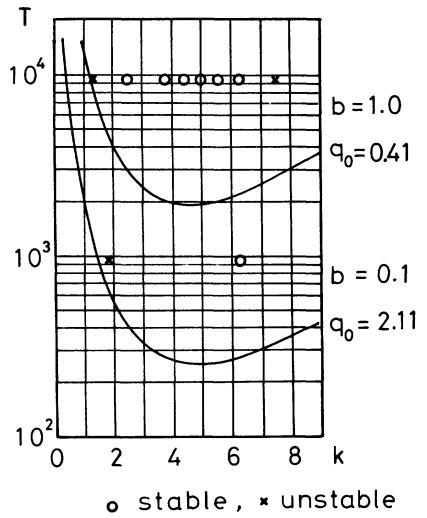

FIG. 7. Stable convective structures. T, electric Rayleigh number; k, wave number; solid lines, obtained from linear stability theory for the quiescent state according to Ref. 9.

erted on each mesh point according to Eq. (A1) with a random force term added to the right-hand side (rhs). The amplitude distributes homogeneously in the range $[-a,a]$, where a was varied from about 0.5 to 80% of the steady maximum value of the vorticity. The results are described below.

1. *Impulsive disturbances*

(a) State A0 was modulated with an impulsive charge disturbance of $k'=2\pi$ and $\Delta q_0=2$, where the other parameter remained constant. At $t=0.5$ the convectional rolls were divided into smaller ones. After fluctuating awhile the system was stabilized at a 12-roll state, as in Fig. 8(a). The final value of the entropy production $P[S]$ did not change signficantly, but the electric current I increased 0.56% from the initial value.

(b) State A10 was modulated with an impulsive disturbance of $k'=1.6\pi$ and $\Delta q_0=2$. The system was stablized at a 12-roll state as in Fig. 8(b).

(c) State A12 was modulated with an impulsive disturbance of $k'=2.2\pi$ and $\Delta q_0=2$. Around $t=1.5$ the system state had become a 16-roll state, then returned back to a 12-roll state [Fig. 8(c)].

(d) State A16 was modulated with an impulsive disturbance of $k'=\pi$ and $\Delta q_0=2$, then changed as in Fig. 8(d) to become a 14-roll state.

(e) State A20 was modulated with an impulsive disturbance of $k'=1.4\pi$ and $q_0=2$, then changed as in Fig. 8(e) to become 14-roll state. The increase of $P[S]$ was about 0.3%.

(f) State A20 was modulated with an impulsive disturbance of $k'=0.4\pi$ and $\Delta q_0=2$, then changed as in Fig. 8(f). Around $t=0.5$ the state was transferred to a state with a wave number of the disturbance. It meant that the disturbance was too strong. The four-roll state was found to be unstable and changed to an eight-roll state. The final values of $P[S]$ and I increased by -0.8 and 0.7%, respectively.

2. *Disturbance by random force*

(g) State A8 was modulated with a random force of $a=5.0$, which corresponds to 20% of the maximum velocity, so called 20% amplitude. The state did not change at 20% amplitude, but changed to a 12-roll state at 80% amplitude as in Fig. 8(g)-2. Variations of I and $P[S]$ were not small. When random force was removed at $t=5.0$ the values converged as in Fig. 8(g)-1.

(h) When A12 was modulated by a random force of 20% amplitude, the structure did not change. When the amplitude of the disturbance was 80% the structure varied as in Fig. 8(h).

(i) When state A16 was modulated with a random force of 80% amplitude, the structure varied and the average size of rolls increased as in Fig. 8(i).

(j) When state A18 was modulated with random force of 0.5% amplitude, the state remained unchanged. When the amplitude was 20% the state changed to a 16-roll state with a 1% increase of $P[S]$ as in Fig. 8(j).

We summarize in Fig. 9 the results of computer simulation of the relative stability among the various metastable states obtained by giving an impulsive perturbation to the initial states, as shown in Figs. 8(a)—8(g). It is evident that a steady convecting system cannot be uniquely specified by the number of rolls or by the wavelength of the rolls, even if the sytem is two dimensional. Therefore, even if the number of rolls is identical between the initial states and the final states, the corresponding currents are not identical. Nevertheless, since the number of the rolls n is a simple parameter, we take it as the horizontal axis of Fig. 9. In the same figure we take the current, which is proportional to the entropy production in a steady state, in the vertical axis, to see the validity of the entropy-production-maximum principle. The open circles are the current corresponding to the initial states obtained from small fluctuations. The transition from an initial state to a final state certainly depends on the character of the perturbation. The examples we show in Fig. 9 are very limited, considering the variety of the possible perturbations one can envisage. Nevertheless, there exists a general tendency for the final state to carry more current than the corresponding initial

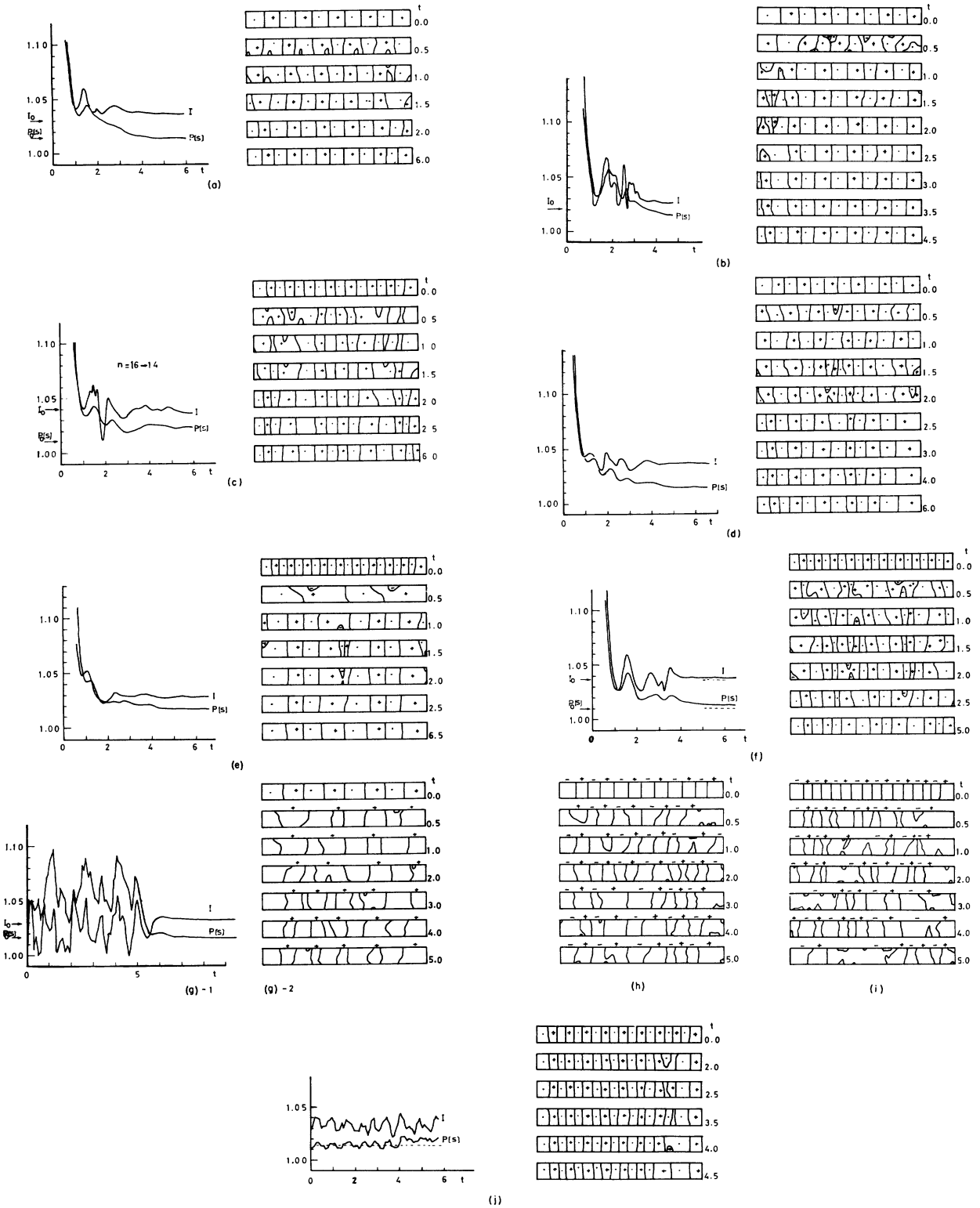

FIG. 8. Evolutions from stable states by disturbances. (a) A0, $k'=2.0\pi$; (b) A10, $k'=1.6\pi$; (c) A12, $k'=2.2\pi$; (d) A16, $k'=\pi$; (e) A20, $k'=1.4\pi$; (f) A20, $k'=0.4\pi$; above for impulsive disturbances; (g) A8, random force with 80% amplitude; (h) A12; (i) A16; and (j) A18 for 20% amplitude.

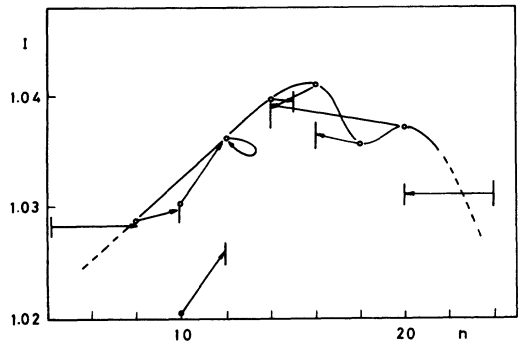

FIG. 9. Transitions from metastable states by disturbances; arrows indicate the initial states and the final states.

one with one notable exception. This is understandable, as this initial state is the one with the maximum current. Any transition from it will decrease the current. These limited results are consistent with the principle of maximum entropy production, although more examples have to be studied.

The final states are obtained by the impulsive perturbation scatter in the region of n from 12 to 16. These results are consistent with the analysis of the data perturbed constantly by a random noise shown in Figs. 8(h) and 8(i). In each disturbed system the distribution of roll size was obtained by measuring the size of rolls appearing at $z=0.5$ and at $t=1$, 2, 3, 4, and 5. The number of appearnces of the roll is plotted as a function of the wave number $2/\lambda$, which is equal to $n/10$. In Fig. 10, (a) and (b) are the initial states and (a') and (b') are the corresponding state during the random perturbation. In this range of calculation the most frequently appearing roll corresponds to 1.2 for $2/\lambda$ or $n=12$, which is the same region with the results of Fig. 9 within the computational error.

E. Numerical errors

In our numerical analysis the accuracy was second order in h in the ω calculation both in time and space, better than first order in space, and first order in time in charge calculation by means of the donor cell method. The numerical errors can be evaluated by comparing the results with either analytical solutions or experimental results. In our problem it was only the quiescent conduction state that was obtained analytically. Numerical results for this state agreed with the analytical solution within 1% in charge density and 0.05% in electric potential. Therefore, the donor cell method used for charge calculation could be regarded to give good results with nearly the above accuracy.

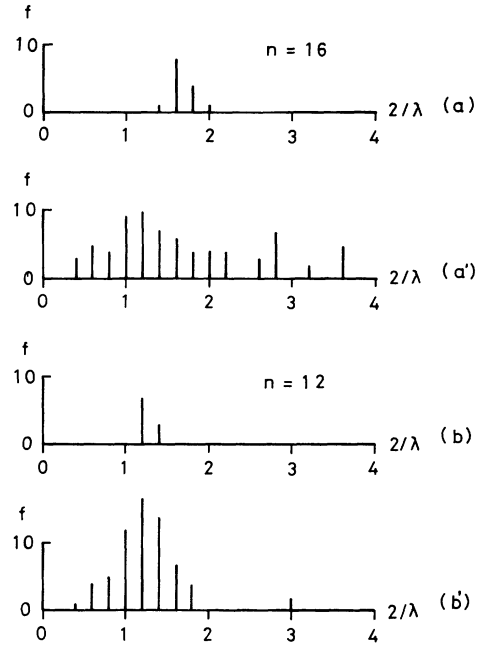

FIG. 10. Variations of the distribution of wave numbers. Horizontal axis is $2/\lambda$, which is equal to $n/10$. Vertical axis is the number of appearances of the rolls of a given wave number. (a) Sixteen-roll state, (a') disturbed as in Fig. 8(i); (b) Twelve-roll state, (b') disturbed as in Fig. 8(h).

Another evaluation was made be comparing the electric current and the entropy production. These values should agree since the input power was all dissipated; however they differed by 2%, so the absolute numerical errors in average current were estimated to be around 2%. However, the profile showing a maximum in Fig. 9 may be justified because the relative error in each convecting state is considered to be less than the absolute error.

IV. CONCLUSION

The electroconvective structure was studied numerically, by finite difference schemes, for the first time with full nonlinearity. The spatial structure and its evolution under the perturbation were examined. The relative stability among the various metastable states was discussed. The central results are summarized as follows:

(1) A quiescent conduction state was obtained in a condition below the critical Rayleigh number which was given by the linear stability theory. The numerical errors were 0.05% in electric potential, 1.0% in charge density, and 0.03% in average current.

(2) In a condition above the critical electric Ray-

leigh number and with some initial perturbations, several regular convective structures were established stably. The region of the wave number for the stable structure was narrower than the line showing the marginal stability of the quiescent state. When initial perturbations with wave numbers near the marginal stability condition were given such perturbations grew for a while, then collapsed and changed to become convective structures with wave numbers relatively more stable. It was found that in the starting state second-order differentials in the current curves with respect to time were negative, while they were positive for the cases achieving stable structures. The numerical error in the convective region was estimated to be around 2% in average current.

(3) In steady stable convective states the liquid velocity and the electric current take maximum values in the region $1.2<\lambda<1.7$, where λ is the wavelength. Although the two maximum wavelengths were slightly different, they were in the same region within the computational errors.

(4) Steady stable convective states were able to be transferred to other states by perturbations. By transitions the system was found to occupy a more efficient state to transport charge or to dissipate energy, consistent with the maximum-entropy-production principle proposed by Sawada[7] and Felici.[6]

ACKNOWLEDGMENTS

The authors greatly appreciate the advice of Professor H. Daiguji in the numerical analysis. They also acknowledge stimulating discussions with Professor Y. Takeuchi, Professor N. Sato, Dr. S. Ohta, Dr. K. Nakajima, H. Honjo, and H. Shimizu. This work was partially supported by a grant from the Ministry of Education, Japan.

APPENDIX

Here the actual process of numerical calculation is described in detail. The vorticity equation, Eq. (8), is written in the Crank-Nicholson method as

$$\begin{aligned}\frac{\omega_{i,j}^{n+1}-\omega_{ij}^{n}}{\Delta t}=&-\frac{1}{2}\frac{\Psi_{i,j+1}-\Psi_{i,j-1}}{2h}\left[\frac{\omega_{i+1,j}^{n+1}-\omega_{i-1,j}^{n+1}}{2h}+\frac{\omega_{i+1,j}^{n}-\omega_{i-1,j}^{n}}{2h}\right]\\&+\frac{1}{2}\frac{\Psi_{i+1,j}-\Psi_{i-1,j}}{2h}\left[\frac{\omega_{i,j+1}^{n+1}-\omega_{i,j-1}^{n+1}}{2h}+\frac{\omega_{i,j+1}^{n}-\omega_{i,j-1}^{n}}{2h}\right]\\&+\frac{1}{2R_e}\left[\frac{\omega_{i+1,j}^{n+1}-2\omega_{i,j}^{n+1}+\omega_{i-1,j}^{n+1}}{h^2}+\frac{\omega_{i+1,j}^{n}-2\omega_{i,j}^{n}+\omega_{i-1,j}^{n}}{h^2}\right]\\&+\frac{1}{R_e}\left[\frac{\omega_{i,j+1}^{n+1}-2\omega_{i,j}^{n+1}+\omega_{i,j-1}^{n+1}}{h^2}+\frac{\omega_{i,j+1}^{n}-2\omega_{i,j}^{n}+\omega_{i-1,j}^{n}}{h^2}\right]\\&-\frac{q_{i,j+1}-q_{i,j-1}}{2h}\frac{\Phi_{i+1,j}-\Phi_{i-1,j}}{2h}+\frac{q_{i+1,j}-q_{i-1,j}}{2h}\frac{\Phi_{i,j+1}-\Phi_{i,j-1}}{2h}\,.\end{aligned}\tag{A1}$$

In the donor cell method the convection term in the above equation becomes

$$\frac{1}{2}\left[\left[-\frac{u_R\omega_R^{n+1}-u_L\omega_L^{n+1}}{h}-\frac{u_T\omega_T^{n+1}-u_B\omega_B^{n+1}}{h}\right]+\left[-\frac{u_R\omega_R^{n}-u_L\omega_L^{n}}{h}-\frac{u_T\omega_T^{n}-u_B\omega_B^{n}}{h}\right]\right],\tag{A2}$$

where

$$\begin{aligned}&u_R=(u_{i+1,j}+u_{i,j})/2,\quad u_L=(u_{i-1,j}+u_{i,j})/2\,,\\&u_T=(u_{i,j+1}+u_{i,j})/2,\quad u_B=(u_{i,j-1}+u_{i,j})/2\,,\\&\omega_R=\omega_{i,j}\ \ (u_R>0),\quad \omega_R=\omega_{i+1,j}\ \ (u_R<0)\,,\\&\omega_L=\omega_{i-1,j}\ \ (u_L>0),\quad \omega_L=\omega_{i,j}\ \ (u_L<0)\,,\\&\omega_T=\omega_{i,j}\ \ (u_T>0),\quad \omega_T=\omega_{i,j+1}\ \ (u_T<0)\,,\\&\omega_B=\omega_{i,j-1}\ \ (u_B>0),\quad \omega_B=\omega_{ij}\ \ (u_B<0)\,.\end{aligned}\tag{A3}$$

$u_{i,j}$'s are obtained from $\Psi_{i,j}$'s by the central difference scheme. For charge density q in the donor cell method Eq. (10) becomes

$$\frac{q_{i,j}^{n+1}-q_{i,j}^{n}}{\Delta t}=-\frac{v_Rq_R-v_Lq_L}{h}-\frac{v_Tq_T-v_Bq_B}{h}\,,\tag{A4}$$

where n denotes time t_n. The rhs is expressed at t_n, and

$$
\begin{aligned}
v_R &= (u_{i+1,j}+u_{i,j}+E_{i+1,j}+E_{i,j})/2 \\
v_L &= (u_{i-1,j}+u_{i,j}+E_{i-1,j}+E_{i,j})/2 \\
v_T &= (u_{i,j+1}+u_{i,j}+E_{i,j+1}+E_{ij})/2 \\
v_B &= (u_{i,j-1}+u_{i,j}+E_{i,j-1}+E_{i,j})/2 \\
q_R &= q_{i,j} \quad (u_R>0), \quad q_R = q_{i+1,j} \quad (u_R<0) \\
q_L &= q_{i-1,j} \quad (u_L>0), \quad q_L = q_{i,j} \quad (u_L<0) \\
q_T &= q_{i,j} \quad (u_T>0), \quad q_T = q_{i,j+1} \quad (u_T<0) \\
q_B &= q_{i,j-1} \quad (u_B>0), \quad q_B = q_{i,j} \quad (u_B<0) .
\end{aligned} \tag{A5}
$$

The stream function Ψ and the electric potential Φ are obtained by solving Poisson equations (9) and (11). These equations become, in the central difference scheme,

$$
(\Psi_{i+1,j}+\Psi_{i-1,j}+\Psi_{i,j+1}+\Psi_{i,j-1}-4\Psi_{i,j})/h^2 = \omega_{i,j} \tag{A6}
$$

$$
(\Phi_{i+1,j}+\Phi_{i-1,j}+\Phi_{i,j+1}+\Phi_{i,j-1}-4\Phi_{i,j})/h^2 = -q_{i,j} . \tag{A7}
$$

A. Boundary conditions

At the rigid boundaries the fluid velocity u is zero. The boundary condition is

$$
\Psi=0 \quad \text{for } z=0,\ z=1,\ x=0, \text{ and } x=10 . \tag{A8}
$$

For ω the boundary values are obtained by extrapolations.

$$
\Psi_{w+1} = \Psi_w + h\frac{d\Psi}{d\xi}\bigg|_w + \frac{h^2}{2!}\frac{d^2\Psi}{d\xi^2}\bigg|_w + \frac{h^3}{3!}\frac{d^3\Psi}{d\xi^3}\bigg|_w + O(h^4) . \tag{A9}
$$

Here Ψ_w is an arbitrary constant at the rigid walls and can be chosen to be zero as in Eq. (A8). The second term in Eq. (A9) vanishes since it is a component of fluid velocity. At the rigid walls the third term is expressed by ω_w according to Eq. (A6), which is $h^2\omega_w/2$. The fourth term then becomes $\partial\omega/\partial\xi\,|_w$, which is in the first-order approximation $(\omega_{w+1}-\omega_w)/h+O(h)$. Therefore,

$$
\omega_w = \frac{3}{h^2}\Psi_{w+1} - \frac{1}{2}\omega_{w+1} + O(h^2) , \tag{A10}
$$

which is called the Wood condition.[15] For charge density q

$$
q = q_0 \quad \text{at } z=0 . \tag{A11}
$$

At the collector ($z=1$) and the side walls ($x=0$ and $x=10$) the values are extrapolated from inner values. Here we use the following extrapolation method:

$$
q_w = 4(q_{w\pm1}+q_{w\pm3}) - 6q_{w\pm z} - q_{w\pm4} \quad \text{at } x=0,\ x=10, \text{ and } z=1 . \tag{A12}
$$

For the electric potential Φ

$$
\Phi = 1 \text{ at } z=0 ,
$$

$$
\Phi = 0 \text{ at } z=1 ,
$$

and

$$
\Phi_w = 4(\Phi_{w\pm1}+\Phi_{w\pm3}) - 6\Phi_{w\pm2} - \Phi_{w\pm4} \quad \text{at } x=0 \text{ and } x=10 . \tag{A13}
$$

The above method is based on an assumption such that the third-order differentials of the extrapolation curves are small and zero at least at $w\pm2$. This assumption is nearly satisifed when the curves have gentle slopes near the walls.

Since the boundary potential Φ_w should be consistent with Eq. (A7), several iterations according to the following computations were made in order to obtain the constant results at each time. The convergence within 10^{-4} to 10^{-5} deviations against 1 were obtained by less than ten iterations.

Each of the dynamic equations for ω and q and Poisson equations for Ψ and Φ was transformed into 891 linear equations, respectively. Generally, such equations are solved by Gauss, Crout, SOR, ADI, and so on.[15] We applied the Crout method, one of direct methods, here.

The quiescent conductive state, which was obtained analytically, plus small perturbations were used as the initial conditions.

B. Evaluation of electric current and entropy production

The transient electric current should be calculated by taking into account not only the migration of space charge, but also the displacement current. We evaluated transient current by taking the mean value at the injector and the collector.

$$
I = \frac{1}{2I_0}\int_0^1 \left[\left[q(x,0)E(x,0) + \frac{\partial E(x,0)}{\partial t} \right] + \left[q(x,1)E(x,1) + \frac{\partial E(x,1)}{\partial t} \right] \right] dt , \tag{A14}
$$

where I_0 is the value corresponding to the quiescent conduction current. At the steady state I becomes equal to the electric Nusselt number. On the other hand, the nondimensional expression of entropy production is given by[16]

$$P[S]=\frac{1}{T_m P_0}\int_V dV[qE_i^2+Tu_{i,k}(u_{i,k}+u_{k,i})]\ , \tag{A15}$$

where T is the electric Rayleigh number and T_m the absolute temperature. The first term of the rhs expresses the dissipation due to the Joule effect and the second term the viscous dissipation. P_0 is the entropy production for the quiescent conduction state with superscripts:

$$P_0=\frac{1}{T_m}\int_V dVq^0E_i^{0^2}\ .$$

*Present address: Mechanical Engineering Laboratory, Ibaraki 305, Japan.

[1]G. Nicolis and I. Prigogine, *Self-Organization in Nonequilibrium Systems* (Wiley, New York, 1977).

[2]P. Glansdorff and I. Prigogine, *Thermodynamic Theory of Structure Stability and Fluctuations* (Wiley, New York, 1971).

[3]R. Landauer, Ann. N. Y. Acad. Sci. 316, 433 (1979).

[4]W. V. R. Malkus and G. Veronis, J. Fluid Mech. 4, 225 (1958).

[5]P. H. Roberts, *Non-equilibrium Thermodynamics, Variational Techniques and Stability,* edited by R. Donnelly, R. Herman, and I. Prigogine (University of Chicago Press, Chicago, 1969), p. 125.

[6]N. J. Felici, C. R. Acad. Sci. 278B, 151 (1974); 278B, 807 (1974).

[7]Y. Sawada, Prog. Theor. Phys. 66, 68 (1981).

[8]N. J. Felici, Rev. Gen. Electr. 78, 717 (1969); Direct Current 12, 24 (1967).

[9]M. Suzuki and Y. Sawada, J. Appl. Phys. 51, 5667 (1980).

[10]For example, T. Teorell, J. Gen. Physiol. 42, 831 (1959), or Y. Kobatake and H. Fujita, J. Chem. Phys. 40, 2212 (1964).

[11]P. Atten and R. Moreau, J. Mec. 11, 471 (1972).

[12]J. M. Schneider and P. K. Watson, Phys. Fluids 13, 1948 (1970).

[13]J. C. Lacroix, Thése de doctorat és-sciences, Grenoble, 1976 (unpublished).

[14]P. Atten and J. C. Lacroix, J. Electrostatics 5, 439 (1978).

[15]P. J. Roache, *Computational Fluid Dynamics* (Hermosa, New Mexico, 1972).

[16]M. Matsushita, J. Phys. Jpn. 41, 674 (1976).